Dynamically Interacting Processes Underlie Synaptic Plasticity in a Feedback Pathway

Anne-Marie M. Oswald, John E. Lewis and Leonard Maler

J Neurophysiol 87:2450-2463, 2002. doi:10.1152/jn.00711.2001

Journal of Neurophysiology publishes original articles on the function of the nervous system. It is published 12 times a year (monthly) by the American Physiological Society, 9650 Rockville Pike, Bethesda MD 20814-3991. ISSN: 0022-3077, ESSN: 1522-1598. Visit our website at http://www.the-aps.org/.

J Neurophysiol
87: 2450–2463, 2002; 10.1152/jn.00711.2001.

Dynamically Interacting Processes Underlie Synaptic Plasticity in a Feedback Pathway

ANNE-MARIE M. OSWALD, JOHN E. LEWIS, AND LEONARD MALER
Department of Cellular and Molecular Medicine, University of Ottawa, Ottawa, Ontario K1H 8M5, Canada

Received 24 August 2001; accepted in final form 13 December 2001

Oswald, Anne-Marie M., John E. Lewis, and Leonard Maler. Dynamically interacting processes underlie synaptic plasticity in a feedback pathway. *J Neurophysiol* 87: 2450–2463, 2002; 10.1152/jn.00711.2001. Descending feedback is a common feature of sensory systems. Characterizing synaptic plasticity in feedback inputs is essential for delineating the role of feedback in sensory processing. In this study, we demonstrate that multiple interacting processes underlie the dynamics of synaptic potentiation in one such sensory feedback pathway. We use field recording and modeling to investigate the interaction between the transient high-magnitude potentiation (200–300%) elicited during tetanic stimulation of the feedback pathway and the lower magnitude posttetanic potentiation (PTP; ~30%) that slowly decays on cessation of the tetanus. The amplitude of the observed transient potentiation is graded with stimulus frequency. In contrast, the induction of PTP has a stimulus frequency threshold between 1 and 5 Hz, and its amplitude is independent of stimulus frequency. We suggest that the threshold for PTP induction may be linked to a minimum level of sustained potentiation (MSP) during repetitive trains of stimuli. We have developed a novel model that describes the interaction between the transient plasticity observed during train stimulation and the generation of PTP. The model combines a multiplicative, facilitation-depression-type (*FD*) model that describes the transient plasticity, with an enzymatic network that describes the dynamics of PTP. The model links transient plasticity to PTP through an input term that reflects MSP. The stratum fibrosum–pyramidal cell (StF-PC) synapse investigated in this study is the terminus of a feedback pathway to the electrosensory lateral line lobe (ELL) of a weakly electric gymnotiform fish. Dynamic plasticity at the StF-PC synapse may contribute to the putative role of this feedback pathway as a sensory searchlight.

INTRODUCTION

In an ever-changing environment, the primary objective of a sensory system is to distinguish relevant stimuli from a noisy background. The Amazonian, brown ghost knife fish, *Apteronotus leptorhynchus*, relies on its electric sense to navigate a complex environment of organic and inorganic matter, find food and mates, and avoid predation. A wide variety of stimuli, including the animal's own movements, other electric fish, and organic and inorganic objects, cause distortion in the fish's electric field. Electroreceptors on the skin surface respond vigorously to these distortions regardless of whether they are caused by reafferent stimuli such as tail movements or by novel stimuli such as prey (Bastian 1981a, 1995).

Electroreceptor afferents project to the electrosensory lateral line lobe (ELL), a hindbrain structure that serves as the first-order processing center for the electric sense. Here they form synapses with the basal dendrites of pyramidal cells (Maler et al. 1974). In addition to receiving afferent input, ELL pyramidal cells also receive feedback input from higher brain centers onto their apical dendrites (Maler et al. 1981).

As the major output neurons of the ELL, the pyramidal cells encode input from a population of electroreceptors (Chacron et al. 2001; Ratnam and Nelson 2000) and transmit it to higher brain centers (Bastian 1981b; Gabbiani et al. 1996). However, unlike electroreceptors, pyramidal cells respond vigorously only to novel electrosensory input, and these responses decay with repeated presentation of the stimulus (Bastian 1995). Thus pyramidal cells act as adaptive filters of predictable input.

It has been shown that this adaptive filtering is, in part, dependent on anti-Hebbian synaptic plasticity between the direct feedback pathway that descends from the nucleus praeminentialis (NPd) via the stratum fibrosum (StF), and the proximal apical dendrites of ELL pyramidal cells (PC) (Bastian 1996a,b, 1998a). Earlier in vivo work has shown that high-frequency (70–100 Hz) trains of stimuli delivered to the StF predominantly result in potentiation of the StF-PC synapse (Bastian 1996b). It has also been shown that the short-term form of plasticity, posttetanic potentiation (PTP), can be readily elicited at StF-PC synapses in vitro and may depend on presynaptic CAMKIIα (Wang and Maler 1997, 1998).

In the present study we identify and characterize multiple forms of short-term plasticity including facilitation, short-term depression, and PTP at StF-PC synapses. We also describe the properties of PTP at these synapses including the stimulation frequency threshold for induction of PTP and the stimulation frequency independent amplitude of PTP. Finally, we have developed a phenomenological model that not only describes the observed transient dynamics of facilitation and depression during train stimulation, but also accounts for both the dynamics and threshold properties of PTP. In doing so we are able to make some suggestions as to the potential role of short-term synaptic plasticity in ELL sensory processing.

METHODS

Transverse brain slices from the ELL of the brown ghost knife fish, *Apteronotus leptorhynchus*, were prepared according to animal care guidelines established by the University of Ottawa and as previously described (Berman et al. 1997). Briefly, the fish were anesthetized

Address for reprint requests: L. Maler, Dept. of Cellular and Molecular Medicine, University of Ottawa, 451 Smyth Rd., Ottawa, Ontario K1H 8M5, Canada (E-mail: lmaler@aix1.uottawa.ca).

The costs of publication of this article were defrayed in part by the payment of page charges. The article must therefore be hereby marked "*advertisement*" in accordance with 18 U.S.C. Section 1734 solely to indicate this fact.

with MS222 and then respirated with oxygenated water containing MS222. The brain stem was removed, glued to a plastic stage, and then immersed in ice-cold artificial cerebrospinal fluid [ACSF, composed of (in mM) 124 NaCl, 24 $NaHCO_4$, 10 D-glucose, 1.25 KH_2PO_4, 2 KCl, 2 $MgSO_4$, and 2 $CaCl_2$; all chemicals from Sigma unless otherwise noted]. ELL slices (350 μm) were cut using a Vibraslice and immediately transferred, rostral side up, to the recording chamber. The slices were then maintained at room temperature (20–22°C) in oxygenated ACSF for 1–2 h prior to recording.

The fibers of the StF are myelinated and appear opaque in relation to the rest of the slice. Thus the StF is an easily identified landmark for the placement of stimulating and recording electrodes. A monopolar tungsten electrode (<5-μm tip diam) was positioned in the medial segment (MS) of the ELL at the dorsal aspect of the StF to preferentially stimulate the excitatory afferents that run dorsally and terminate in the ventral molecular layer (VML) (Berman et al. 1997; Mathieson and Maler 1988). Stimulus timing was computer controlled (Igor Pro, Wavemetrics and Pulse Control) (Herrington et al. 1995), and delivered as 20- to 40-μs pulses of 20–35 V through a stimulus isolation unit (Digitimer, Herts, England). Stimulation intensity was determined as that which produced maximal paired-pulse facilitation, based on two stimulus pulses delivered 50 ms apart yet remained subthreshold for action potential generation. This permitted measurement of field excitatory postsynaptic potentials (EPSPs) during train stimulation without contamination by action potentials or their after-hyperpolarizations.

Baseline stimulation consisted of single or paired pulses (50 ms apart) delivered at 0.1 Hz for ≤18 min. Tetanic stimulation was delivered as 10 10-pulse trains with a 1-s intertrain interval. Train frequency varied from 1, 5, 50, or 100 Hz. Test pulses (single or paired) were delivered in the 1 s between the trains at 500 ms.

Field potentials were recorded using 3- to 10-MΩ borosilicate glass electrodes (Brown-Flaming P-87, Sutter Instruments), filled with ACSF and positioned in the VML of the centromedial segment (CMS). After a stable baseline was obtained, tetanic stimulation was applied, and the transient long-term effect of the tetanus on EPSP amplitude was assessed by test pulses delivered every 10 s for 15 min starting 5 s after the last train.

Data analysis

Field potentials were amplified and low-pass filtered (3 kHz; Axoclamp 2A, Axon Instruments, Burlingame CA), digitized (Instrutech, Greatneck, NY), and stored for analysis (Igor Pro and Pulse Control). Analysis was done with IgorPro. Statistical significance was assessed by ANOVA. All results are reported as means ± SE unless otherwise stated.

Model description

In this paper, we discuss two qualitatively distinct forms of short term synaptic enhancement (transient *facilitation*- and *depression*-like processes, on the order of milliseconds and seconds, and a *posttetanic potentiation*, PTP, on the order of minutes). In this light, our model follows two distinct formalisms. Facilitation and depression are modeled by a previously described formalism for short-term synaptic plasticity (Dittman et al. 2000; Fischer et al. 1997; Magleby and Zengel 1975; Varela et al. 1997). We refer to this as the *FD* model, and summarize it briefly below. This type of model is sufficient for describing the short-term facilitation and depression in both the direct and indirect feedback pathways to ELL (Lewis et al. 2000). However, *FD* models are not capable of explaining the combination of short-term and longer term plasticity described in the present study because the long time constants required for the slow decay (of PTP for example) would result in synaptic enhancement under control stimulation conditions (i.e., in the absence of a tetanus). Therefore a different formalism must be used to explain synaptic enhancement on the longer time scales. We build on the traditional *FD* model by describing PTP with two additional variables, X_P and Y_P, whose dynamics are given by a set of coupled ordinary differential equations similar to those described in enzymatic networks (for example, see Matsushita et al. 1995).

In the *FD* model, a postsynaptic potential (PSP) due to a brief stimulus pulse is given by the combination of a number of processes that can either increase (*F* processes) or decrease (*D* processes) the PSP relative to its control value (A_0). In preliminary analyses we found that four different processes (F_1, F_2, D_1, and D_2) were required to adequately fit the *FD* model to the PSPs during the stimulus trains. After each stimulus arrives, the values of F_i and D_i change by a discrete amount, the update magnitude (*Eq. 1*)

$$F_1 \rightarrow f_1 + F_1$$
$$F_2 \rightarrow f_2 + F_2$$
$$D_1 \rightarrow [1 - d_1(F_1 - 1)] \cdot D_1$$
$$D_2 \rightarrow d_2 \cdot D_2 \quad (1)$$

The update magnitude for the D_1 process is related to F_1, similar to previous studies (Dittman et al. 2000; Hempel et al. 2000). This was required to account for the range of responses that were observed across the different frequencies tested. Between stimuli, F_i and D_i decay exponentially to a value of one with their respective time constants (*Eq. 2*)

$$\tau_{F_i} \frac{dF_i}{dt} = 1 - F_i$$
$$\tau_{D_i} \frac{dD_i}{dt} = 1 - D_i \quad (2)$$

The posttrain dynamics of PTP were described by a qualitatively different process, F_{PTP}. The variables X_P and Y_P, whose dynamics are described in *Eq. 3*, dictate the dynamics of F_{PTP} (*Eq. 4*)

$$\tau_x \frac{dX_P}{dt} = \frac{(w_1 X_P - Y_P)^2}{k^2 + (w_1 X_P - Y_P)^2} - X_P$$
$$\tau_Y \frac{dY_P}{dt} = w_2 X_P - Y_P \quad (3)$$
$$F_{PTP} = 1 + w_3 Y_P \quad (4)$$

At each stimulus, X_P is perturbed by an amount *S* (*Eq. 5*). The process described by *S* shows dynamics similar to those of F_2 in the current formulation (*Eq. 6*)

$$X_P \rightarrow S + X_P \quad (5)$$
$$S \rightarrow s_o + S$$
$$\tau_S \frac{dS}{dt} = -S \quad (6)$$

The overall responses of the model to stimulation are given by a combination of five different processes (*Eq. 7*), as in previous studies (Fischer et al. 1997)

$$\mathrm{PSP} = A_0 \cdot (F_1 + F_2) \cdot D_1 \cdot D_2 \cdot F_{PTP} \quad (7)$$

Initially the model was fit to mean 5- and 50-Hz data sequentially, and Table 1 shows the list of model parameters and the values that fit these stimulus protocols. An asterisk next to the parameter indicates that the parameter was fitted by least-squares, otherwise parameter values were fixed at constant values. The data from 1 and 100 Hz were not used for this initial fit. With these parameter values (Table 1), the root-mean-squared (RMS) errors for each of the four frequencies (1, 5, 50, and 100 Hz) were 5.4, 6.1, 5.4, and 17.2%, respectively. In

TABLE 1. *Model parameters*

Parameter	Value	LS Fit
f_1	1.814	*
τF_1	0.0211	*
f_2	0.435	*
τF_2	0.903	*
d_1	0.0567	*
τD_1	1.35	*
d_2	0.995	*
τD_2	8.85	*
k	0.5	
w_1	1.2	
w_2	0.25	
w_3	2.00	*
τ_x	10	
τ_y	130	
s_o	0.004	
τ_s	1.2	

LS, "least squares" fit. *, fitted parameters.

addition to fitting the mean data, we also performed least-squares fits of the model to data from individual slices where both 50- and 100-Hz stimulation were performed (see RESULTS). In these fits, most parameters were constrained to the values shown in Table 1. Initially, the 50-Hz data were fit with the free parameters being f_1, f_2, d_1, d_2, and w_3. From these fits, it was apparent that the values of f_1 and d_1 had the highest variability; the coefficients of variation for each of the five parameters were 0.46, 0.35, 0.54, 0.002, and 0.29, respectively. We then tested whether the 100-Hz data could be explained by changes in only f_1 and d_1 by fitting the data from both 50- and 100-Hz stimulation with only these two parameters free to vary, and the remaining three parameters fixed to the values found in the 50-Hz fits. In six of eight cases, varying the values of these two parameters could explain a large part of the differences between the 50- and 100-Hz data (RMS error $<$15%). Table 2 shows how these parameters changed between the fits to the 50- and 100-Hz data (also see RESULTS).

RESULTS

The direct feedback pathway connects the ELL and the nucleus praeminentialis (Pd; Fig. 1). Briefly, pyramidal cells project axons to the Pd, activating stellate cells (glutamatergic) and bipolar cells (GABAergic). The stellate cells and bipolar cells then project back to the ELL via the stratum fibrosum (StF) and synapse on the spines of the proximal apical dendrites of pyramidal cells and the soma, respectively. In addition, local ELL interneurons, namely stellate cells and VML cells, receive direct excitatory input from StF fibers resulting in disynaptic inhibition through interneuron-pyramidal cell synapses.

Stimulation of the StF evoked field potentials similar to

TABLE 2. *Summary of 50-Hz/100-Hz comparison*

Parameter	Mean Value
50 Hz f_1	1.8 ± 0.83
50 Hz d_1	0.057 ± 0.031
Parameter	Mean % Difference from 50-Hz Value
100 Hz f_1	37 ± 41
100 Hz d_1	290 ± 212

Values are means ± SD.

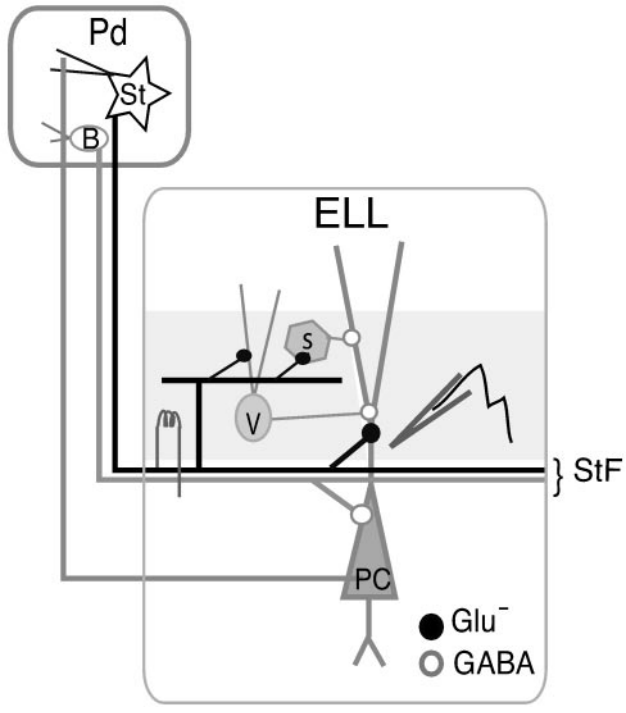

FIG. 1. Circuitry of the direct feedback pathway. The direct feedback circuit is part of a closed loop between the nucleus praeminentialis (Pd) and the electrosensory lateral line lobe (ELL). Pyramidal cell (PC) axons contact Pd stellate cells (St) and bipolar cells (B). The axons of the stellate and bipolar cells form the excitatory and inhibitory tracts, respectively, of the stratum fibrosum (StF). The StF then closes the feedback loop by making excitatory (Glu^-, glutatmate) and inhibitory (GABAergic) connections on the apical dendrites and soma of the PCs. In addition, excitatory fibers also synapse with local ELL interneurons, ventral molecular layer (VML) cells (V) and stellate cells (s), which make inhibitory contacts with PCs. In the slice preparation, the StF was stimulated in the medial segment of the ELL, and field recordings were taken in the ventral molecular layer (shaded) of the centromedial segment.

those previously described (Berman et al. 1997; Wang and Maler 1997). The biphasic field potential had a brief positivity that was often obscured by the fiber volley, followed by a larger negativity with an amplitude of 0.4–1.5 mV depending on stimulus intensity; the latency to peak of this negativity was ~5.5 ms (5.45 ± 1.01 ms, mean ± SD; Fig. 2*A*). Previous studies using current source density (CSD), intracellular recording, and pharmacological analysis have demonstrated that this negativity represents StF-evoked compound EPSPs (Berman et al. 1997). As in previous studies (Varela et al. 1997), we utilize field recordings to reduce the damage caused by intracellular impalement, which allows long-term recording at the same site enabling us to compare different stimulation frequencies. We have confirmed our results with a small number of intracellular recordings ($n = 5$, data not shown).

Baseline StF stimulation, consisting of single or paired pulses delivered every 10 s for ≤18 min did not result in potentiation of field EPSPs (99.11 ± 2.44%, mean ± SE). As previously reported (Wang and Maler 1997, 1998), fiber volleys at all stimulation frequencies, either transiently decreased (<10%) or did not change during the trains. Following the trains, volleys changed slightly (±5 ± 2%) or did not change at all. Since the potentiation of EPSP amplitudes is consistent regardless of the small positive or negative changes in fiber volley, it is unlikely that a change in fiber volley contributes significantly to the 20% to >300% changes in EPSP amplitude. In a few slices ($n = 4$) the fiber

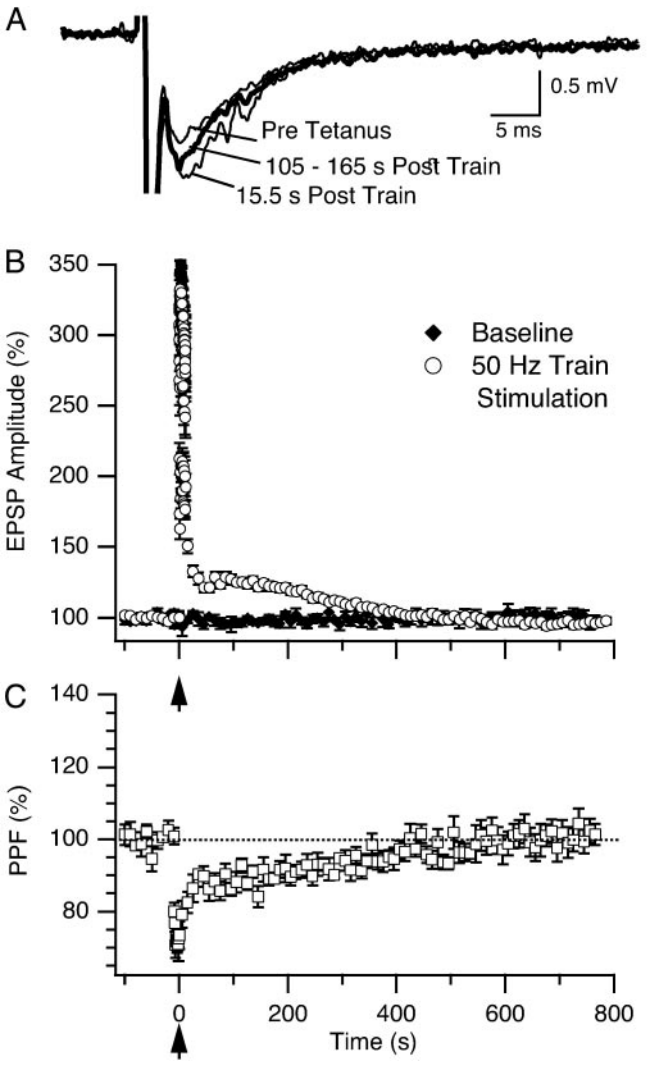

FIG. 2. Short-term synaptic plasticity in StF-PC synapses. Stimulation of the StF with 10 50-Hz trains (delivered at arrow) resulted in a large transient potentiation during the trains followed by a smaller slowly decaying potentiation on train cessation. *A*: field excitatory postsynaptic potentials (EPSPs) taken from the VML in response to StF stimulation. Pretetanus trace: thick black line, average of 10 baseline pulses (0.01 Hz). Posttetanus traces: thin black line, single trace taken 15.5 s after trains cessation; thick gray trace, average of 5 traces (10 s apart) during stable phase of posttetanic potentiation (PTP) decay, 105–165 s posttetanus. *B*: mean response ($n = 19$ slices) to 50-Hz train stimulation. EPSP amplitudes (○) are reported as a percentage of pretrain baseline values, error bars SE. EPSP amplitudes remain significantly different from baseline values (◆) for ≤260 s following train cessation (* $P < 0.01$). *C*: paired-pulse facilitation (PPF) in response to same protocol in *B*. PPF values are presented as a percentage of pretrain baseline values. Reduction in PPF is maximal during train stimulation, and PPF values return to baseline with a time course similar to PTP.

volleys increased ≤20% following train stimulation. In these cases, the EPSP was fused to the fiber volley, and these measurements were likely contaminated. Consequently, these slices were not included in the present analysis.

Potentiation in response to train stimulation at varying frequencies

A total of 28 slices was studied. Of these slices, 25 demonstrated short-term synaptic potentiation in response to tetanic stimulation without significant change in fiber volley, and 3 were excluded from analysis due to depression during and following train stimulation. Of the 25 slices that potentiated, 19 showed a sustained (~5 min) potentiation following cessation of the tetanus.

Tetanic stimulation consisted of 10 10-pulse trains of varying frequencies with 1 s between trains. This burst type protocol mimics the in vivo firing pattern of the Pd stellate cells that give rise to the StF fibers. On excitation, the normally quiet satellite cells produce short bursts of activity that have an average frequency of 80 Hz over a 100-ms period (Bratton and Bastian 1990). However, as will be shown in this paper, higher frequencies of train stimulation lead to increasingly variable responses during stimulation; thus our standard frequency of stimulation during the trains was 50 Hz.

Tetanic stimulation of the StF with 50-Hz trains resulted in a large mean transient increase in EPSP amplitudes during train stimulation (328 ± 24%; Fig. 2*B*). This transient potentiation decayed to 151 ± 5% within 5 s of train cessation. Following this, EPSP amplitudes plateaued for ~2 min around 124 ± 3%. The EPSPs remained significantly potentiated over baseline values for 4.3 min ($P < 0.01$) after train cessation (Fig. 2*B*). The decay from 5 s posttetanus to baseline was fit with a single exponential with a τ value of 6.19 min. This τ value is suggestive of PTP as seen in other systems (see Fischer et al. 1997 for review).

In six experiments, single test pulses were replaced with paired pulses, 50 ms apart, to ascertain the possible locus of the potentiation. During baseline stimulation, there was an average paired-pulse facilitation (PPF) of 176 ± 10%. During train stimulation PPF was reduced to 125 ± 4%. Following the trains, there was a significant sustained reduction in PPF (153 ± 8%, 5 min; $P < 0.01$). All PPF values were then normalized to the mean baseline PPF value (Fig. 2*C*). Following the trains, the reduction in PPF returned to baseline levels with a similar time course to PTP (Fig. 2*C*). These reductions in PPF suggest that the likely source of both transient potentiation and PTP is a presynaptic increase in synaptic efficacy (for review see Zucker 1989).

In trials where train stimulation was changed to 1, 5, or 100 Hz, tetanic stimulation of the StF resulted in graded degrees of potentiation during the trains of stimuli that was dependent on stimulation frequency (Fig. 3). The mean transient potentiation during the trains had maximum amplitudes of 136 ± 8% (1 Hz, $n = 6$, Fig. 3*A*) and 200 ± 20% (5 Hz, $n = 7$, Fig. 3*B*). Interestingly, during the 100-Hz trains, the mean maximum potentiation is less (231 ± 36%, $n = 8$) than that during 50 Hz (compare Fig. 2*B* and Fig. 3*C*).

In contrast to the transient potentiation during the trains that were stimulation frequency dependent, 5- and 100-Hz stimulation resulted in a level of PTP comparable with that seen at 50 Hz, suggesting that the amplitude of PTP is stimulation frequency independent. The maximum posttrain amplitudes (at 5 s) were 152 ± 6% (5 Hz) and 151 ± 5% (100 Hz). The amplitudes of the plateau potentiations were 133 ± 6% (5 Hz) and 126 ± 4% (100 Hz; Fig. 3, *B* and *C*). These amplitudes were not significantly different from those seen with 50-Hz stimulation. The τ-values of PTP decay were 6.81 min (5 Hz) and 5.49 min (100 Hz). Like the results seen at 50 Hz, both 5- and 100-Hz stimulation resulted in decreased PPF during the trains as well as sustained reduction in PPF following the trains (data not shown).

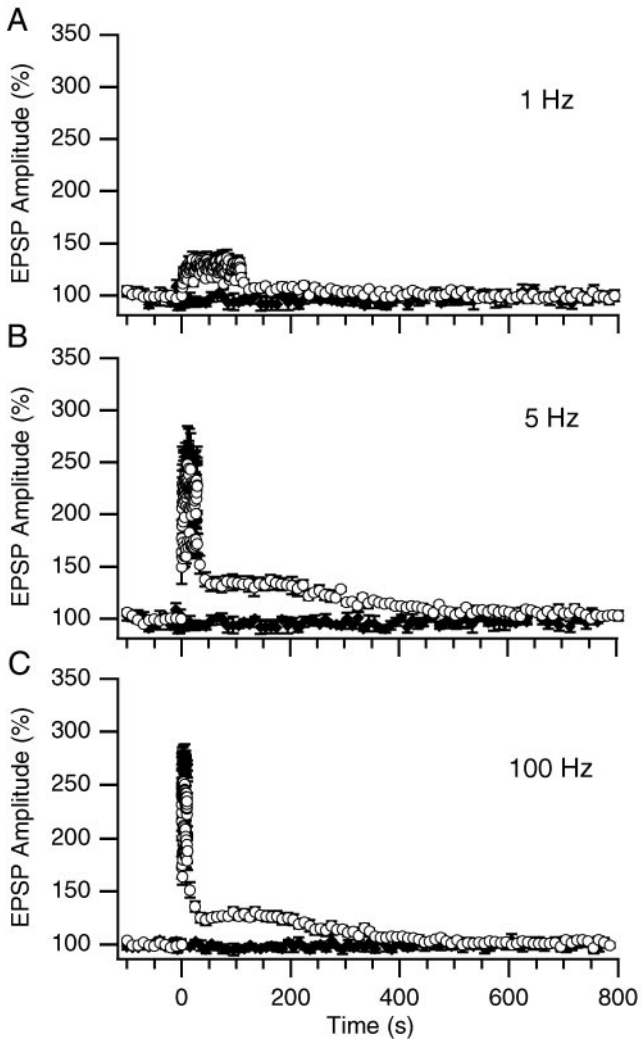

FIG. 3. Frequency-dependent changes in short-term synaptic plasticity at StF-PC synapses. Mean responses to 10 10-pulse trains of 1, 5, and 100 Hz during tetanic stimulation. EPSP amplitudes (○, mean ± SE) for all frequencies are reported as percentage of pretrain baseline values. *A*: during 1-Hz trains, there is minimal transient potentiation (<140%) and no demonstrable PTP following the trains. *B* and *C*: 5- and 100-Hz train stimulation resulted in 200–250% transient potentiation, followed by PTP with amplitude and decay characteristics similar to that reported following 50-Hz trains (Fig. 2*B*).

It is important to note that 1-Hz train stimulation did not produce PTP as neither the maximum amplitude (112 ± 5%) nor the average amplitude (105 ± 3%) following the trains was significantly different from baseline values (maximum: 105 ± 5%, average 98 ± 3%; Fig. 3*A*). Nor was there a significant reduction in PPF following train cessation (pretrain: 165 ± 5%; posttrain: 159 ± 5%).

Determining the PTP data set

In a small number of slices (6), train stimulation at 50 Hz resulted in transient potentiation during the trains but failed to produce long-lasting PTP (Fig. 4*A*). The mean maximum amplitude at 5-s posttrain was 112 ± 7%, and the mean plateau amplitude was 108 ± 5%. PPF decreased by 30% during the trains but only demonstrated a significant reduction in PPF at 5 s posttetanus ($P < 0.01$; Fig. 4*B*).

These results, in conjunction with the 1-Hz data set, suggest that quantitative criteria are required to distinguish slices in which PTP is elicited from those where it is not. We developed a procedure to quantify PTP following the trains; a similar method has been described previously (Jensen et al. 1999). This procedure takes into account both the duration and amplitude of PTP. The first step was to establish a point when the potentiation would be considered recovered. The baseline EPSP amplitudes are normalized to 100% and vary with a SD of 9%. Thus we set 109% as our "recovery amplitude." We then found the first point at which the smoothed decay curve crossed 109% and set that time point as "recovered." We then

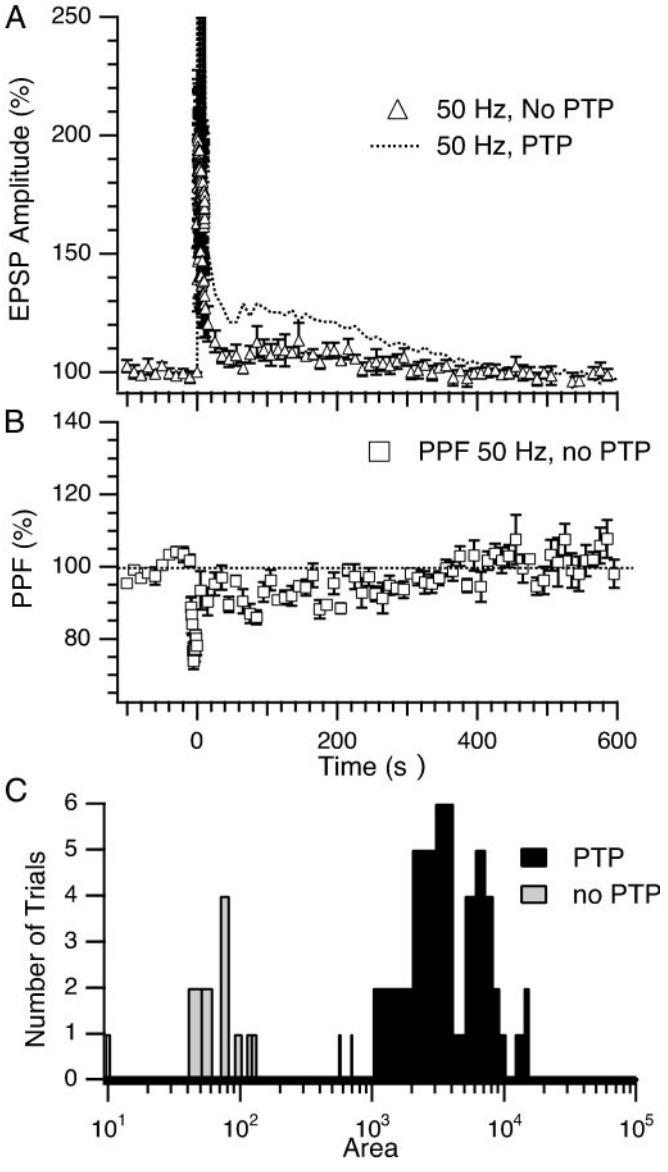

FIG. 4. Comparison of PTP trials vs. no PTP trials. *A*: in 6 slices, 50-Hz stimulation did not yield PTP (△). Dotted line represents mean PTP in response to 50-Hz stimulation. *B*: PPF following the trains in non-PTP trials was not significantly different from baseline values. *C*: areas under the decay curves following train cessation were assessed in all trials. Briefly, the decay curves were smoothed from 5-s posttrains to 720 s. The area was then measured to the point where the decay curve 1st crossed 109% (established by baseline variation). A bimodal distribution of the data set is evident with trials that demonstrated PTP (most 5- and 50-Hz data; filled bars, areas >1,000) and trials (a few trials at 5 and 50 Hz, as well as all 1-Hz data) that did not demonstrate PTP, no-PTP (shaded bars, areas ≤100).

took the area under the decay curve from 5 s posttrain to the recovered time point. This resulted in a bimodal data set of "PTP" versus "no-PTP" trials, where PTP trials had areas of 1,000 or greater and no-PTP trials had areas <100 (Fig. 4*C*). Only slices that had areas that met the PTP criteria were used for analysis and modeling.

Minimum sustained potentiation

In comparing the two data sets PTP and no-PTP, as defined by our assessment of area under the decay curve (Fig. 4*C*), there appears to be a minimum level of potentiation sustained during train stimulation in the PTP set that is not sustained in the no-PTP set. To determine a value for this minimum sustained potentiation (MSP), the sustained potentiation in each trial was quantified and the MSP for the PTP data set was ascertained. Briefly, the EPSP amplitude at the first pulse of each train (with the exception of the 1st train) is the remaining potentiation from the previous train summed with the current stimulus. This serves to estimate the level of potentiation sustained between trains. Thus for each individual trial the amplitude of first pulse of each train (excluding the 1st train) was measured as a percentage of the mean baseline stimulation value. These amplitudes were then averaged, and the mean value represents the sustained potentiation for that trial. In all cases that demonstrate PTP (trains of 5 to 100 Hz) the sustained potentiation during train stimulation is $\geq 150 \pm 6\%$ (determined as the mean sustained potentiation during 5-Hz trains). It is possible that this level may indicate a threshold for PTP generation since the sustained potentiation during 1-Hz trains (no PTP) is $122 \pm 4\%$, and only $127 \pm 3\%$ in non-PTP trials of higher frequencies. Both of these values are significantly different from sustained potentiation at 5 Hz ($P < 0.05$) and 50 Hz (MSP = $170 \pm 4\%$; $P < 0.01$; Fig. 5*A*). We suggest that it is the *minimum* sustained potentiation during the trains that must surpass a threshold for PTP rather than the maximum potentiation (measured as the mean of the peak amplitudes of each train) for two reasons. First, the mean maximum potentiation at 5 Hz ($200 \pm 20\%$) is significantly less ($P < 0.01$) than 50 Hz ($328 \pm 24\%$), but 5-Hz stimulation still elicits PTP. Second the mean maximum potentiation of the 5-Hz set is not significantly different from that of the no-PTP set ($179 \pm 13\%$), yet 5-Hz stimulation yields PTP while the latter does not (Fig. 5*B*). When sustained potentiation is plotted against the area under the PTP decay curve, there is a distinct clustering of points for the PTP and no-PTP trials (Fig. 5*C*). These results suggest that the MSP is related to the threshold for the induction of PTP.

Modeling short-term enhancement in the ELL

In looking at the EPSP amplitudes attained during 50-Hz train stimulation, it is evident that multiple processes contribute to StF-pyramidal cell (PC) plasticity (shown schematically in Fig. 6). During train stimulation, two facilitation processes are apparent. The first (*line 1*) has a fast onset that rapidly increases EPSP amplitude within the first two or three stimuli of each individual train. The second (*line 2*) process builds slowly and seems to plateau by the third train. There also appear to be two depression processes; a fast depression that reduces EPSP amplitudes during the last few stimuli of individual trains (*line 3*), and a slower one that becomes apparent during the later trains of the tetanus (*line 4*). Following train stimulation, at least one more process, PTP is evident.

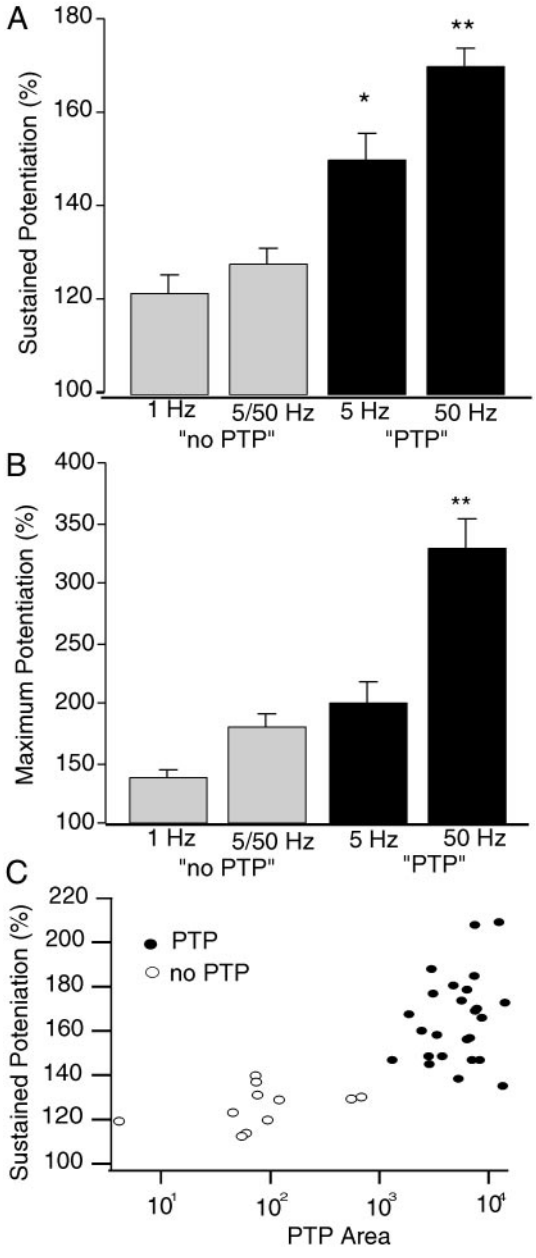

FIG. 5. Minimum sustained potentiation (MSP) during train stimulation. *A*: the sustained potentiation (%) during train stimulation measured as the mean of the amplitudes of the 1st EPSP of each train (except the 1st train). The sustained potentiation in the no-PTP trials (gray bars, 1 Hz, 5 Hz/50 Hz "no PTP") was significantly less than PTP trials (black bars, 5 Hz and 50 Hz "PTP"; error bars: SE). The sustained potentiation during 50-Hz stimulation was significantly less than 5 Hz ($P < 0.05$) and the no PTP trials (** $P < 0.01$). The sustained potentiation during the 5-Hz PTP trials was significantly greater than the no-PTP trials (* $P < 0.05$), suggesting the MSP for PTP induction is $\geq 150\%$. *B*: maximum potentiation (%; mean of the peak EPSP amplitudes of each train). Only 50-Hz stimulation during the PTP trials demonstrated maximum potentiation that was significantly different from the other trials (** $P < 0.01$). *C*: sustained potentiation (%) plotted against the areas under the decay curves for PTP (●) and no-PTP (○) trials. There is a distinct clustering of points for the PTP and no-PTP cases.

To describe the rapid kinetics of the transient potentiation during train stimulation as well as the more complex dynamics

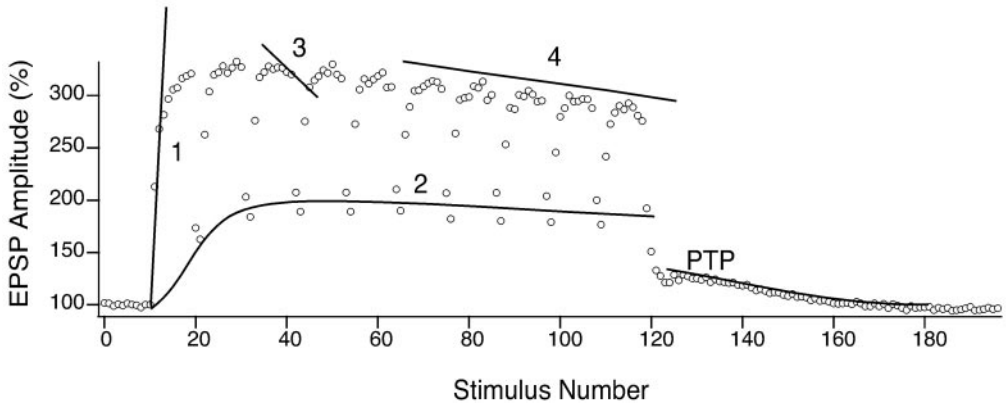

FIG. 6. Schematic of plasticity at the StF-PC synapse with 50-Hz stimulation. EPSP amplitude vs. stimulus number for the mean 50-Hz data set. Five trends are apparent and shown schematically. During the trains, there appear to be 2 potentiating trends; one that is maximal within the 1st few pulses of each train (*1*) and another that builds more slowly and is sustained across the trains (*2*). There also appear to be 2 trends that decrease potentiation: one that decreases EPSP amplitudes during individual trains (*3*) and a 2nd that builds during later trains (*4*). Finally a 5th trend (PTP) decays slowly on cessation of train stimulation.

of PTP, we developed a phenomenological model that combines two approaches: we used the previously proposed facilitation and depression (*FD*) models (Dittman et al. 2000; Lewis et al. 2000; Magleby and Zengel 1975; Varela et al. 1997) together with coupled differential equations that describe enzymatic networks (Matsushita et al. 1995). The model comprises five processes and is summarized in the following equation (for model details see METHODS)

$$\mathrm{PSP} = A_0 \cdot (F_1 + F_2) \cdot D_1 \cdot D_2 \cdot F_{PTP}$$

In this model, the amplitude (PSP) of the EPSP due to a stimulus is the product of processes that either increase EPSP amplitude ($F_1 + F_2$, F_{PTP}) or decrease the EPSP amplitude (D_1, D_2). A_o refers to the baseline EPSP amplitude prior to tetanic stimulation and, up until now, has been presented as 100%. However, in further discussion of the model, all EPSP data will be normalized to a baseline value of 1, thus this term (A_o) can be omitted.

Generally, the contribution of each process in an *FD* model (F_1, F_2, D_1, D_2) to the PSP is dependent on the timing of the stimuli, the decay constant for each process as well as the incremental increase/decrease of each process with stimulation (referred to here as the update magnitude; *Eq. 1*, METHODS). However, in the case of D_1, the incremental decrease is linked to the F_1 process. A number of *FD* models link fast depression terms to fast facilitation (Dittman et al. 2000; Hempel et al. 2000). In these cases, fast depression is due to vesicle depletion, which can be accelerated by facilitation depending on the probability of release at the synapse. While the probability of release at the StF synapse is unknown, we have found that the frequency dependent potentiation during the trains is also best fit by linking D_1 to F_1 (*Eqs. 1* and *2*, METHODS).

Since the 5- and 50-Hz data sets were more consistent than the 100-Hz data, the model was initially fit to mean 5- and 50-Hz data sequentially to yield parameter values for each plasticity process. All values resulting from this fit are presented in Table 1. The τ values of the fit to mean 5- and 50-Hz data were then fixed and the update magnitudes were allowed to vary while model was refit to all individual data sets at all stimulation frequencies. Although all simulations include all five plasticity processes, the following summary presents model simulation results in two sections: transient potentiation during train stimulation and PTP during and following train stimulation.

Transient potentiation during train stimulation

Simulations of pyramidal cell responses to train input suggest that the majority of the potentiation could be attributed to the contributions of the first four processes. Figure 7 shows the model performance compared with the mean train data at all frequencies tested (parameter values in Table 1). For the 1-Hz data, the model adequately simulated the nominal increases in EPSP amplitudes (Fig. 7*A*). At 5 and 50 Hz, the model nearly perfectly simulated the mean EPSP amplitudes obtained experimentally (Fig. 7, *B* and *C*). However, the model overestimates the average amount of potentiation in response to 100-Hz train stimulation (Fig. 7*D*). It is possible that the variability seen in the 100-Hz data set could bias the mean and could thus affect the interpretation of this comparison. In the next section, we investigate this possibility further.

HIGHER FREQUENCY STIMULATION PRODUCES VARIABLE RESULTS DURING TRAIN STIMULATION. To better assess the variable levels of potentiation observed during 100-Hz stimulation, we analyzed experiments that directly compare 50- and 100-Hz stimulation in the same slice ($n = 8$). In comparing the mean EPSP amplitudes during 50- and 100-Hz stimulation (Fig. 8*A*), it is apparent that on average, 100-Hz stimulation results in less potentiation than 50-Hz stimulation (⊗, Fig. 8*B*). When the maximum potentiation (mean of the peak potentiations in each of the 10 trains) during tetanus was measured in individual experiments, it was found that in five of eight slices, potentiation during 100-Hz tetanic stimulation was less than that seen with 50 Hz (Fig. 8*B*, —). Of the remaining three slices, two showed potentiation with 100-Hz trains slightly greater than that seen at 50 Hz, while one slice demonstrated far greater potentiation during 100-Hz stimulation than 50-Hz stimulation (Fig. 8*B*, · · ·).

The variable and unpredictable results observed with 100-Hz stimulation provided an interesting challenge to the model. As seen in Fig. 7, the model poorly simulates the mean 100-Hz data set. However, by fixing the τ values of F_1, F_2, D_1, and D_2

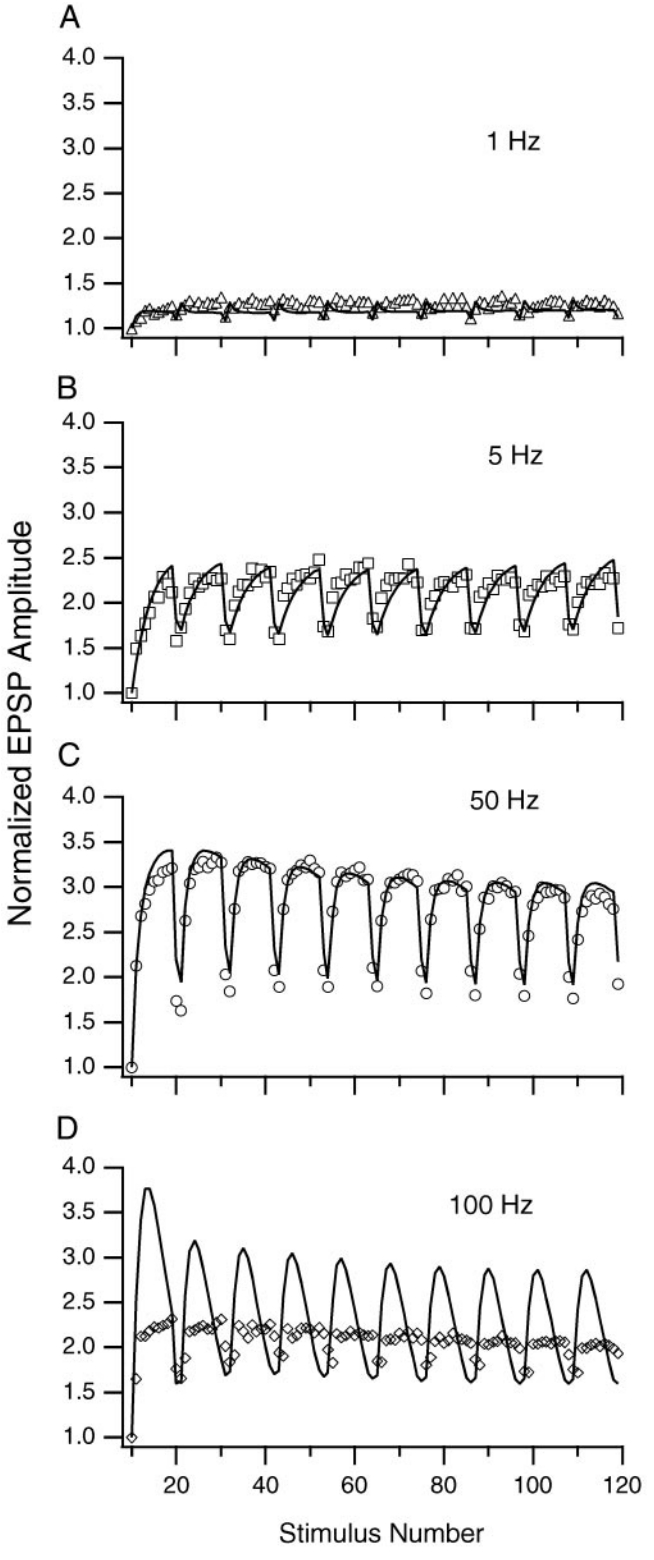

FIG. 7. Experimental and simulated transient potentiation during train stimulation. Experimental EPSP amplitudes (mean data, open symbols) during 1-Hz (*A*), 5-Hz (*B*), 50-Hz (*C*), and 100-Hz (*D*) trains, plotted against stimulus number and normalized to the 1st EPSP of the 1st train. Solid lines represent the simulated EPSP amplitudes based on the $(F_1 + F_2)D_1D_2F_{PTP}$ model. Note that, although the responses are discrete, a continuous line is used for clarity (a similar convention is used for all other figures showing model simulations). The τ-values and update magnitudes for each frequency are reported in Table 1. root-mean-squared (RMS) errors for each frequency are 5.4% (1 Hz), 6.1% (5 Hz), 5.4% (50 Hz), and 17.2% (100 Hz).

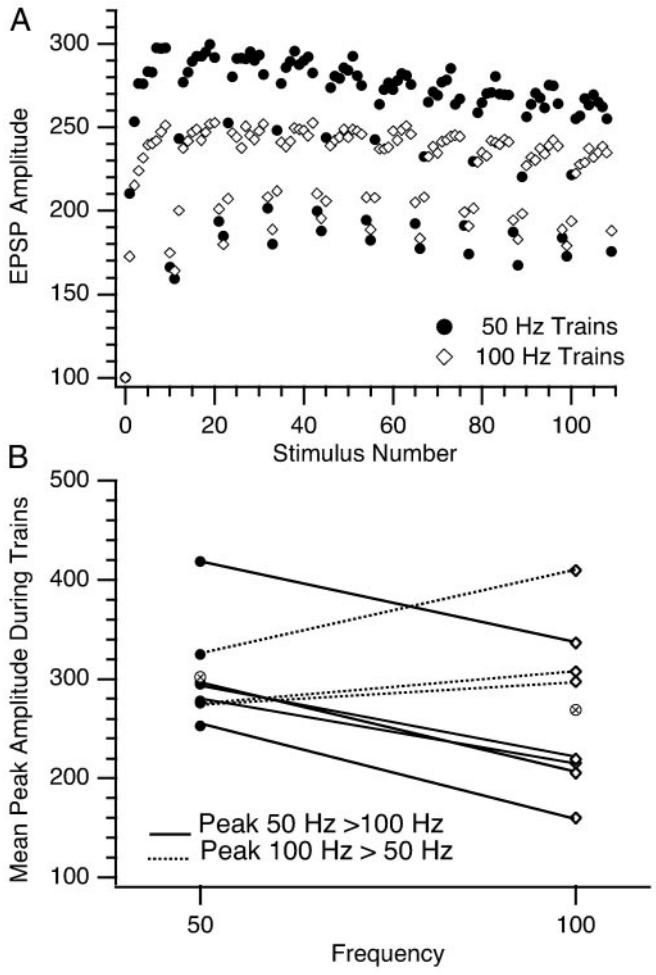

FIG. 8. A slice-by-slice comparison of 50-Hz vs. 100-Hz train stimulation. *A*: the mean EPSP amplitude (% baseline) during 50-Hz trains (●) and 100-Hz trains (◇) are plotted against stimulus number. *B*: a comparison of the maximum amplitude (% baseline) obtained during 50-Hz (●) and 100-Hz (◇) train stimulation in the same slice. In 5 slices, 100-Hz stimulation resulted in a higher maximum amplitude than 50 Hz (—), and in 3 slices 100-Hz potentiation resulted in lower maximum amplitude (· · ·). The mean values are also plotted (⊗) and, as seen in *A*, the mean maximum for 100 Hz is <50 Hz. Note the broader range of values obtained during 100-Hz stimulation.

and leaving the update magnitudes (f_1, f_2, d_1, and d_2) free, the model was able to fit the individual data sets for both 50 and 100 Hz. In comparing the values of the increments, it was found that in the 100-Hz data sets, f_1 and d_1 departed the most from mean 50-Hz values (Table 2). To test whether the variation in the f_1 and d_1 values was sufficient to explain the variation in the 100-Hz data set, we fixed all τ-values (Table 1), we set f_2 and d_2 to mean values for both frequencies, and we left f_1 and d_1 free. We then refit the individual 50- and 100-Hz data sets (see METHODS). Figure 9 shows the experimental results of two slices illustrating the qualitatively different responses to 50- and 100-Hz stimulation. In both slices, as well as in four of the remaining six slices, the model was able to adequately describe the experimental results (RMS error <15%). This suggests that the variation seen at 100 Hz can be explained by a change in the gain of the underlying mechanisms of F_1 and D_1. However, further work will be required to determine the source of this variation.

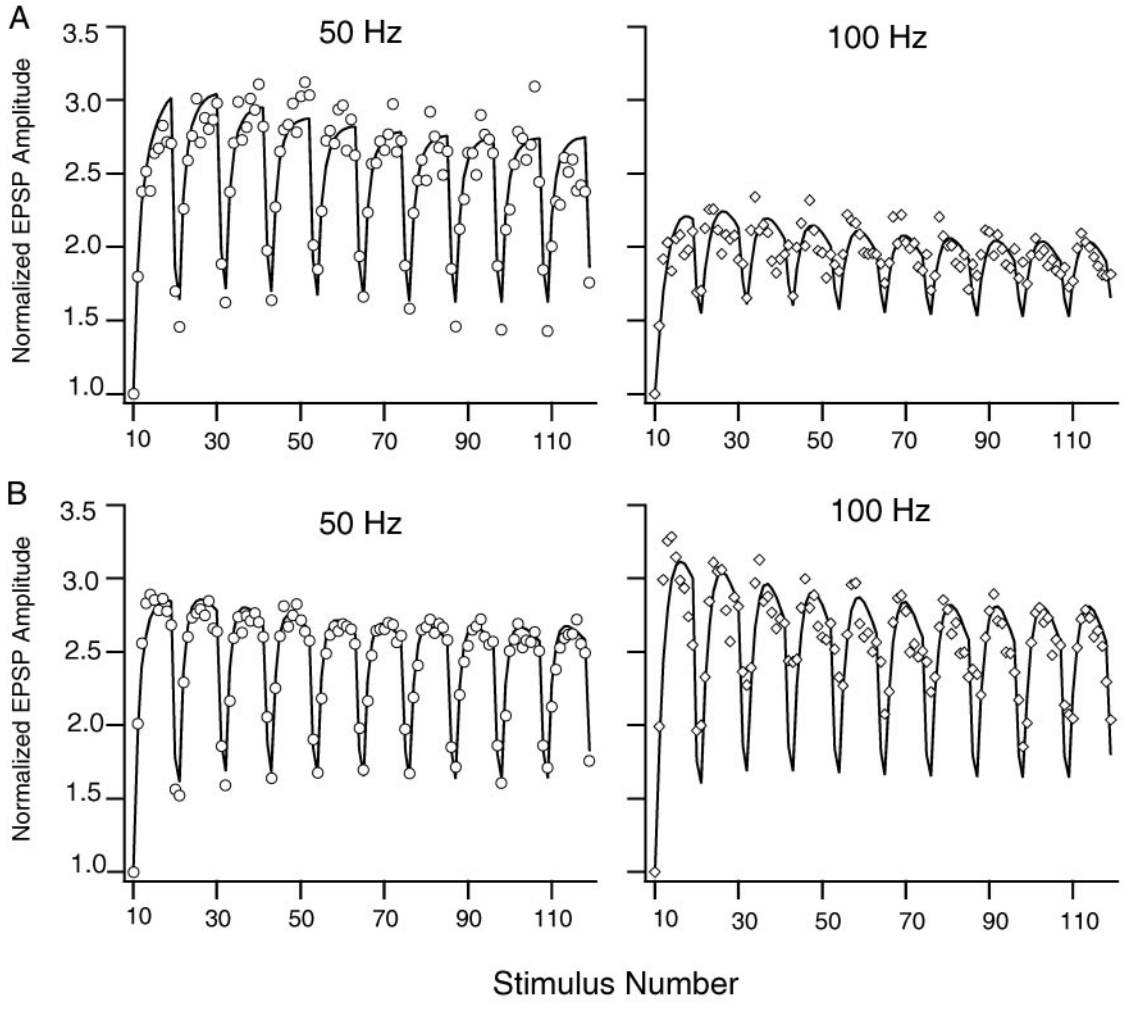

FIG. 9. The variable results of individual slices in response to 100-Hz stimulation. EPSP amplitudes during 50-Hz (○) and 100-Hz (◇) train stimulation in 2 different slices are plotted against stimulus number. The solid lines represent model simulations. To achieve the fits, the τ-values were fixed and the update magnitudes were allowed to vary. *A*: 50-Hz stimulation resulted in greater potentiation than 100-Hz stimulation. Fits: τ-values: Table 1, $f_2 = 0.281$, $d_2 = 0.9956$, $w_3 = 1.985$ for both 50 Hz and 100 Hz and $f_1 = 1.55$, $d_1 = 0.0439$ (50 Hz) and $f_1 = 0.212$, $d_1 = 0.221$ (100 Hz). RMS errors are 6.6 and 8.0% for 50 and 100 Hz, respectively. *B*: 100-Hz stimulation resulted in greater potentiation than 50 Hz. Fits: τ-values: Table 1, $f_2 = 0.292$, $d_2 = 0.9968$, $w_3 = 1.638$ for both 50 and 100 Hz and $f_1 = 1.74$, $d_1 = 0.054$ (50 Hz) and $f_1 = 0.95$, $d_1 = 0.0488$ (100 Hz). RMS errors are 5.7 and 9.7% for 50 and 100 Hz, respectively.

PTP during and following train stimulation

The long time constant required to describe the decay of PTP observed ($\tau \cong 6$ min), prohibits its description by an FD model-type process because it would result in synaptic enhancement with baseline stimulation. This is not seen experimentally (baseline: 99.11 ± 2.44%), and further, PTP is not elicited by 1-Hz trains but maximally elicited by trains above 5 Hz. Hence the model should account for both the frequency threshold of PTP induction during train stimulation as well as the frequency independence of the amplitude of PTP following train cessation.

Both requirements for describing the dynamics of PTP can be achieved using a set of coupled differential equations that are similar to those used to describe enzymatic networks (see METHODS). The network is driven by a stimulus term, *S*, which links the induction of PTP to the amount of enhancement sustained during train stimulation (MSP). These coupled first-order differential equations represent the simplest class of model capable of accounting for both the threshold and constant amplitude of PTP.

Previous studies have localized calcium-calmodulin kinase IIα (CAMKIIα) to StF fibers and verified that StF-evoked PTP can be blocked by the CAMKIIα inhibitor, KN-62 (Maler and Hincke 1999; Wang and Maler 1998). CAMKIIα is a multimeric enzyme that is able to autophosphorylate its individual subunits and remain active following the decay of a calcium signal (Hanson and Schulman 1992). Autophosphorylation is a cooperative, frequency-dependent process. Calcium pulses must initially arrive close enough together for the cooperative binding of calcium calmodulin to the kinase to occur and for autophosphorylation to occur in excess of dephosphorylation by phosphatases (Hanson et al. 1994). Our simplified enzymatic network is based on an interactive activation (X_P) and deactivation (Y_P) relationship that would be suggested by the interaction between CAMKIIα and a phosphatase. We

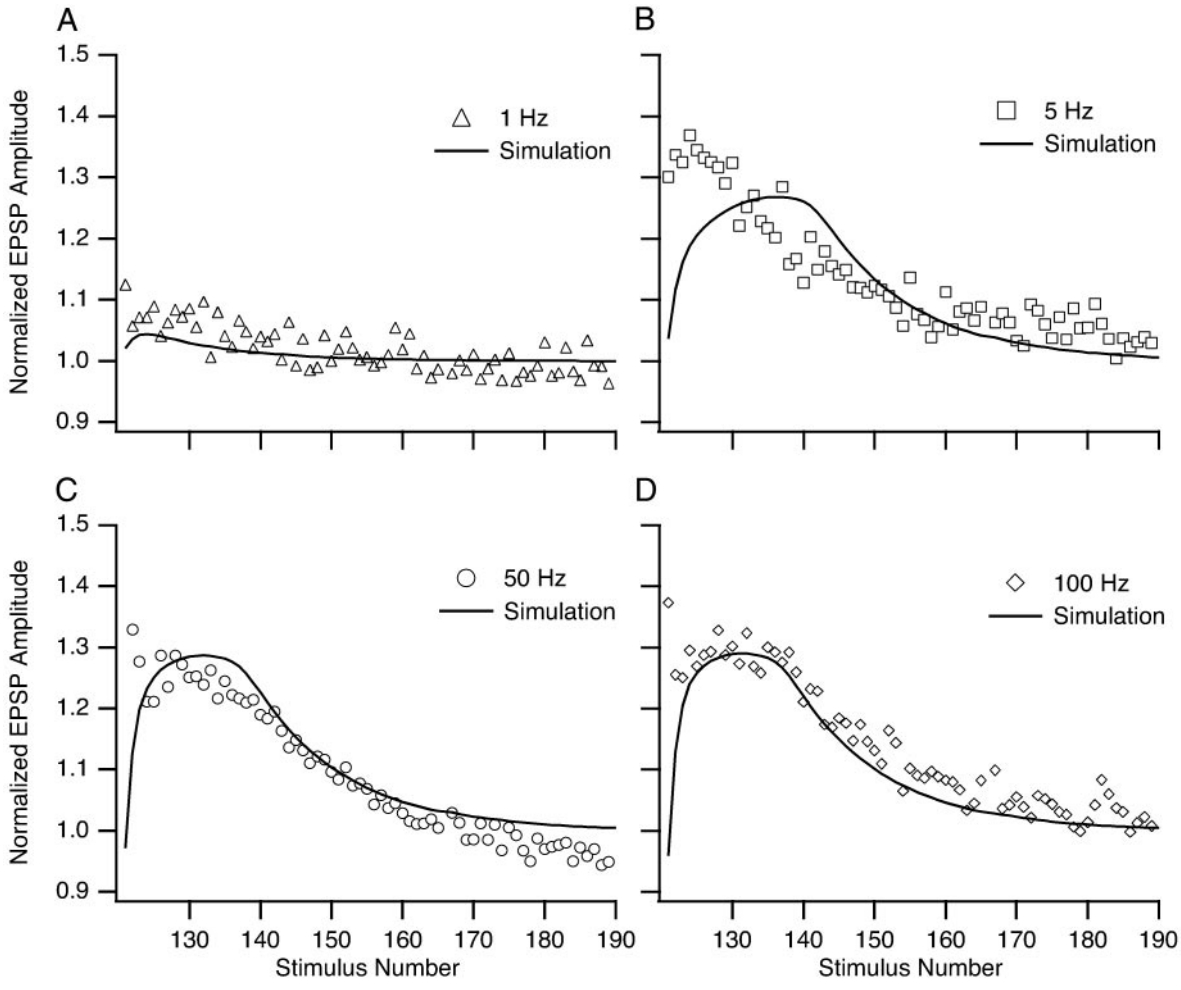

FIG. 10. Experimental and simulated PTP following train cessation. Experimental EPSP amplitudes during the decay of PTP following 1-Hz (*A*), 5-Hz (*B*), 50-Hz (*C*), and 100-Hz (*D*) trains, plotted against stimulus number and normalized to the pretrain baseline values. Solid lines are the simulated EPSP amplitudes based on the $(F_1 + F_2)D_1D_2F_{PTP}$ model (see Table 1 for τ-values and update magnitudes). The model adequately describes the amplitude and time course of PTP following all frequencies of stimulation with the exception of the 1st few points on train cessation.

have added the assumption that X_P is able to autoactivate in a manner similar to CAMKIIα autophosphorylation. When X_P receives the stimulus-related signal (S) from an external source, the activation of X_P results in the autoactivation of X_P as well as the forward activation of Y_P. Once activated, Y_P negatively feeds back to deactivate X_P. The dynamics of X_P and Y_P were modeled using coupled differential equations (see *Eqs. 3* and *4* and METHODS for details).

Characteristics of S: the link between transient potentiation and PTP

The requirements for MSP during the trains have already been described. It is possible that at least one of the transient potentiation processes, F_1 or F_2, is responsible for producing MSP that surpasses the threshold for PTP induction. It has been shown that a minimum level of potentiation must be sustained between trains for the induction of PTP. Since the τ-decay for F_1 is extremely short (21 ms), the incremental increase in EPSP amplitude due to F_1 decays completely during the 1-s intervals between the trains; thus F_1 cannot be a source of sustained potentiation. However, F_2 has a much longer τ (903 ms), and could therefore contribute significantly to sustained potentiation between test pulses. However, although F_2 may be correlated with PTP, we do not have any direct evidence that F_2 is a causal factor in producing PTP. Therefore S is described by an *FD*-type process with dynamics comparable with those of F_2 (*Eqs. 5* and *6* and METHODS).

The model adequately describes PTP at all frequencies (1–100 Hz) except for the first few points following the trains, which are underestimated (Fig. 10). During this time, there is a dip in simulated amplitudes due to the fast offset of F_1 and F_2 compounded with the longer lasting effects of D_2. However, this underestimation is carried on somewhat longer at 5 Hz (Fig. 10*B*). This may be because the experimental EPSP amplitudes during PTP following 5-Hz stimulation were slightly higher than following 50- or 100-Hz stimulation, whereas the model shows a PTP amplitude that is slightly less following 5-Hz stimulation. Alternatively, a fourth short-term, posttetanic enhancement process, augmentation, might be required to explain these data. Augmentation typically has a decay constant in the 10-s to 1-min range and has also been attributed to

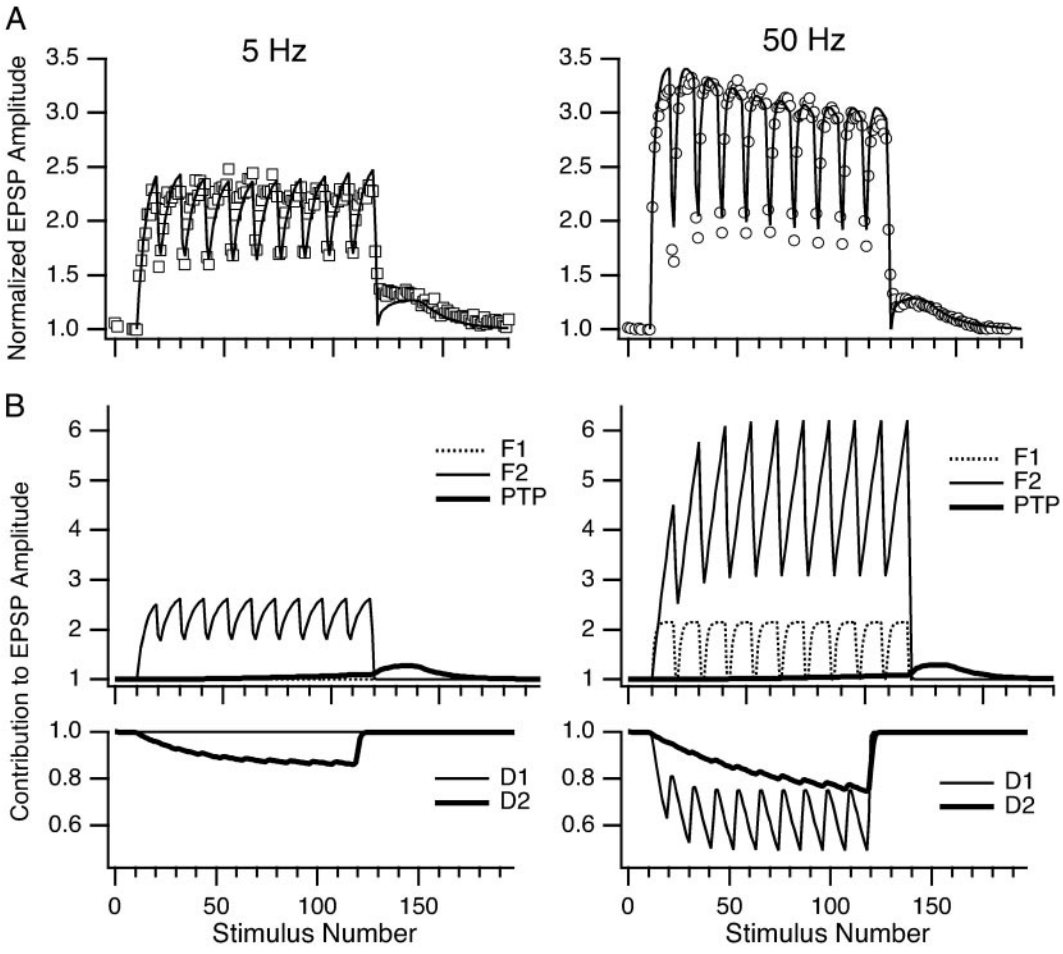

FIG. 11. Summary of experimental and simulated results for 5- and 50-Hz train stimulation. *A*: mean experimental EPSP amplitudes (open symbols) to 5- and 50-Hz stimulation plotted against stimulus number. Simulated fits (solid lines) adequately account for both the frequency-dependent, high-amplitude transient potentiation during trains as well as the frequency-independent, low-amplitude decay of PTP following the trains. *B*: the relative contributions of each variable in the $(F_1 + F_2)D_1D_2\,F_{PTP}$ model to the EPSP amplitude at each point. Note that F_1 and D_1 contribute little during 5-Hz trains but significantly at 50 Hz. Also note that F_2 is the main contributor to EPSP amplitudes during train stimulation.

residual calcium (Fischer et al. 1997). The 170% decay that occurs over the course of the first 15 s following a 50-Hz tetanus is in direct contrast to the rapid decay predicted by model simulations. This suggests that incorporating an augmentation process, with a τ value intermediary of F_2 and F_{PTP}, into the model may account for the underestimation of potentiation directly following the trains. Our protocol, which delivers test pulses 10 s apart following train stimulation, does not enable us to adequately assess the fast decay of a putative augmentation process following the tetanus. We therefore, in the interest of simplicity, did not include an augmentation process into our model.

Figure 11 summarizes the model for both STP and PTP as compared with mean experimental results from 5- and 50-Hz stimulation. It also shows the relative contribution of each plasticity process modeled (F_1, F_2, D_1, D_2, F_{PTP}) at each stimulus (Fig. 11*B*). Note that F_1 and D_1 contribute relatively little to the amplitudes observed during the trains at 5 Hz, but make significant contributions at 50 Hz. The recruitment of these processes at different frequencies may have implications for the function of feedback over the short-duration bursts of activity produced by the stellate cells. However, also note the slow onset of PTP during the trains and that the contribution of F_{PTP} remains relatively constant regardless of frequency (above 5 Hz).

DISCUSSION

This study demonstrates that tetanic stimulation of the StF results in a large, transient potentiation of EPSP amplitudes during train stimulation. The amplitude of this potentiation was frequency dependent between 1 and 100 Hz, and increased EPSP amplitudes up to threefold at the optimal frequency tested (50 Hz). Following the trains, a smaller, slowly decaying potentiation was observed and referred to as PTP because its decay constant (~6 min) is comparable with those reported for PTP in other systems (Fischer et al. 1997). The induction of PTP has a frequency threshold between 1 and 5 Hz but the amplitude of PTP is frequency independent. Experimental evidence suggests that surpassing the threshold for PTP induction depends on the MSP during the trains. Paired-pulse analysis suggests that the locus of both transient potentiation and PTP is presynaptic.

We have developed a model that describes both the transient

potentiation during the trains and the slowly decaying PTP following the trains. Based on the results obtained both experimentally and through simulations, we suggest that at least five overlapping processes contribute to synaptic plasticity at the StF-PC synapse.

Short-term processes during train stimulation

FACILITATION. The high-amplitude transient potentiation during the trains is frequency dependent and can be primarily attributed to short-term facilitation (F_1, F_2). The τ values for F_1 (21 ms) and F_2 (903 ms) are comparable with values for fast decaying facilitation (F_1) and slow decaying facilitation (F_2) in other systems (Fischer et al. 1997). Therefore given the putative presynaptic locus, the enhancement of EPSP amplitudes during F_1 and F_2 facilitation is most likely due to residual calcium in the presynaptic terminal (Delaney and Tank 1994; Zucker 1989).

DEPRESSION. There are also two depression-like processes apparent during train stimulation, D_1 and D_2. The fast depression described by D_1 could be due to vesicle depletion, which, in a number of systems, is a source of short-term depression with a decay constant of 1–2 s (Dittman and Regher 1998; Varela et al. 1999). The extent of vesicle depletion depends on the probability of release at a given synapse, and often, the interplay between depletion, short-term facilitation, and/or the decay of residual calcium in the nerve terminal. Although these parameters have not been established in the ELL, vesicle depletion remains a possible mechanism for D_1.

Alternatively, D_1 may be due to disynaptic GABAergic inhibition. StF fibers make direct excitatory feedback connections onto GABAergic interneurons that synapse onto the apical dendrites and bodies of pyramidal cells. The StF-interneuron synapse could be potentiated in a manner similar to StF-PC synapses resulting in enhanced inhibition through the interneuron-PC synapses (Berman and Maler 1998b; Maler et al. 1981).

The longer time constant of D_2 suggests two other possibilities. Previous studies have demonstrated frequency-dependent, direct inhibitory feedback through the StF to pyramidal cells. These $GABA_B$ IPSPs last $\leq$800 ms and reach peak amplitudes following 100-Hz train stimulation (Berman and Maler 1998a). Alternatively, in in vivo experiments where ELL pyramidal cells are loaded with a calcium chelator, train stimulation of the StF results in significantly greater potentiation than that seen in unloaded cells (Bastian 1998b, 1999). This suggests that there may be calcium-dependent, postsynaptic depression at this synapse, similar to that which has been demonstrated in the mormyrid ELL (Han et al. 2000).

Short-term enhancement: PTP

Following train stimulation, PTP decays over a 6- to 7-min period and is of much lower amplitude (20–30% enhancement) than the transient potentiation. The amplitude of PTP is similar to the amplitude of potentiation reported in previous in vitro (Wang and Maler 1997, 1998) and in vivo experiments (Bastian 1998a). The induction of PTP has a frequency threshold between 1 and 5 Hz. However, the lack of frequency dependence in the amplitude and decay constant of PTP is distinct from other systems, such as the neuromuscular junction, where these values increase with the frequency and duration of the stimulus (Fischer et al. 1997; Magleby and Zengel 1975).

In cultured hippocampal neurons, the amplitude of PTP of GABAergic inhibitory postsynaptic currents (IPSCs) has been shown to be frequency independent above 5 Hz (Jensen et al. 1999). Furthermore, similar to our results, this study demonstrated a frequency threshold for the induction of PTP between 2.5 and 5 Hz. These results suggest that the characteristics of PTP in the ELL (frequency threshold, and frequency independent amplitude) may be found in other brain regions.

Threshold for PTP: a possible role for CAMKIIα

The mechanism of the frequency threshold is unknown. According to PPF analysis, PTP has a presynaptic locus. It has been shown that PTP is linearly correlated with the decay of presynaptic residual calcium but cannot be explained solely by this decay, suggesting that calcium may be acting at a secondary locus (Delaney et al. 1989). We propose that presynaptic residual calcium may be activating an enzyme such as CAMKIIα.

In the ELL, CAMKIIα has been localized to StF fibers (Maler and Hincke 1999), and StF-induced PTP is blocked by the bath application CAMKIIα inhibitor, KN-62 (Wang and Maler 1998). Previous in vitro experiments demonstrate CAMKIIα autophosphorylation in response to calcium pulses delivered at frequencies as low as 4 Hz, leading to nearly maximal autonomous levels of kinase activity (De Koninck and Schulman 1998). Interestingly, 1-Hz pulses did not result in significant amounts of autophosphorylation or autonomous activity. These results attractively parallel the frequency dependence for PTP induction observed in this study.

Autophosphorylation of CAMKIIα is a calcium-dependent cooperative process (Hanson and Schulman 1992); this suggests that a minimum level of calcium must be sustained during tetanic stimulation to induce autonomous activity and, by extension, changes in synaptic efficacy. Although the calcium dynamics of ELL synapses are unknown, the level of transient enhancement during the trains, which can be mainly attributed to residual calcium, might serve as an indirect indicator of the calcium level in the presynaptic boutons.

MSP, the link between transient potentiation and PTP

The results of this paper suggest that a MSP during train stimulation is required for PTP induction. This is based on three observations. First, trials that demonstrate PTP sustain a minimum level of potentiation during the trains that is greater than trials that do not demonstrate PTP. Second, the maximum level of potentiation during the trains does not differentiate PTP and non-PTP trials below 50 Hz. Third, a number of trials reach maximum levels of potentiation during individual trains that surpass the minimum levels predicted for PTP induction; however, this potentiation is not sustained between the trains, and these trials do not demonstrate PTP.

Our results suggest that the minimum level of potentiation is sustained between the trains spaced 1 s apart. Only F_2, with a decay constant of nearly 1 s, can carry the "memory" of one train to the next. However, we cannot be sure of a direct dependence of PTP on the level of potentiation due to F_2. Consequently, for modeling purposes we have defined another

term, *S*, with the dynamics and time constant similar to F_2. We hypothesize that either F_2 is identical to *S*, or that both terms are initiated by a common underlying process. In this way, *S* is able to act as an indicator of MSP during transient potentiation and drive the induction of PTP in our model.

Modeling short-term plasticity in the ELL

In this study, we have taken a novel approach to describe the five processes (F_1, F_2, PTP, D_1, and D_2) underlying the dynamics of short-term plasticity at the StF-PC synapse. F_1, F_2, D_1, and D_2 have been modeled as exponentially decaying *FD*-type processes (Varela et al. 1997). The more complex dynamics of PTP were modeled by an enzymatic network interaction between an autoactivatable kinase, such as CAMKIIα, and a phosphatase. Most importantly, the threshold PTP induction was linked to MSP during train stimulation, through *S*, an F_2-like process.

The completed model exhibits both the modest potentiation seen during the 1-Hz trains, and the frequency-dependent transient potentiation observed at 5–100 Hz. The model also shows the observed threshold between 1 and 5 Hz for PTP induction, and the frequency-independent amplitudes of PTP demonstrated above 5 Hz. This novel combination of modeling approaches has enabled us to describe the synaptic dynamics of the StF-PC synapse and provide a quantitative description of the relative contribution each synaptic process at various stimulation frequencies. These constraints will be useful in determining the underlying causes of plasticity and enable the investigation of potential functions of synaptic plasticity in network models involving closed loop feedback to the ELL.

Functional significance of short-term synaptic plasticity in ELL processing

It has been proposed that the direct feedback pathway acts as a sensory searchlight that enhances the detection of weak signals. The differences in amplitude and duration of potentiation attained during transient potentiation versus PTP suggest that these forms of plasticity may have different roles in this type of ELL processing.

A closely related species of knife-fish, *Apteronotus albifrons*, is able to capture prey in $<$1 s after detection (Nelson and MacIver 1999). Depending on the speed the fish is swimming, the transdermal voltage change across an individual electroreceptor lasts ~200 ms, corresponding to a change in peak firing rate of electroreceptor afferents of 1 or 2 spikes in 60 (Ratnam and Nelson 2000). However, the ability of the fish to detect and capture prey suggests that pyramidal cells must be able to encode such minute changes in firing rate.

It has been suggested that synaptic plasticity of the direct feedback pathway could function as part of a sensory searchlight that could enhance pyramidal cell function (Bratton and Bastian 1990). The searchlight hypothesis was first proposed by Crick (1984), in relation to the visual system. This theory has been updated and described in reference to ELL (Berman et al. 1997). One requirement of the theory is reciprocal excitatory connectivity. This is fulfilled by the reciprocal and topographic positive feedback loop between the ELL pyramidal cells and the Pd stellate cells. A second requirement, nonlinearity in the responsiveness of the pyramidal cells, could be fulfilled by the voltage dependence of pyramidal cell EPSPs, which is likely due to the activation of persistent Na^+ channels on pyramidal cell somata and dendrites (Berman et al. 2001). This voltage-dependent, nonlinearity could result in a supralinear summation of EPSPs.

In their paper, Berman et al. (1997) hypothesized that "when electroreceptor and StF input arrive concurrently at a pyramidal cell, the StF input is enhanced greatly and therefore is very effective at bringing the cell above spike threshold." In the current study, we have shown that trains of 50 Hz or greater delivered to the StF are able to transiently enhance pyramidal cell EPSP amplitudes up to threefold in 100–200 ms. Furthermore, the most significant changes in EPSP amplitude occur within the first 20–100 ms of train stimulation. In the intact animal, the feedback through the StF has a delay of ~20–30 ms (Berman et al. 1997; J. Bastian, personal communication). These time frames suggest that in addition to the voltage dependence of EPSPs (Berman et al. 1997, 2001), transient potentiation (F_1 and F_2 facilitation specifically) of the direct feedback pathway could rapidly and dramatically potentiate the sensory searchlight. The combination of synaptic enhancement and EPSP voltage dependence might conservatively be expected to produce $>$400% increases in StF EPSP amplitudes; this would be expected to greatly enhance electroreceptor input as the fish advances toward its prey. The topographic nature of the StF feedback pathway implies that this enhancement is confined to pyramidal cells adjoining those activated by electroreceptor input; thus the transient potentiation demonstrated in this paper is likely to contribute to the detection of the weak signals caused by prey objects.

Conversely, the duration of PTP extends longer than expected for prey capture. However, in a more complex environment, such as the tangled root masses of the flooded Amazon River basin (Crampton 1998), a more persistent up-regulation of the sensory searchlight may be necessary during scanning and foraging behavior (Lannoo and Lannoo 1992).

We thank B. Doiron for helpful discussions.

This work was supported by a grant from the Canadian Institutes for Health Research (CIHR) to L. Maler, a CIHR postdoctoral fellowship to J. E. Lewis, and an Ontario Graduate Scholarship (ST) to A.-M.M. Oswald.

REFERENCES

BASTIAN J. Electrolocation I. How the electroreceptors of *Apteronotus albifrons* code for moving objects and other electrical stimuli. *J Comp Physiol [A]* 144: 465–479, 1981a.

BASTIAN J. Electrolocation II. The effects of moving objects and other electrical stimuli on the activities of two categories of posterior lateral line lobe cells in *Apteronotus albifrons*. *J Comp Physiol [A]* 144: 481–494, 1981b.

BASTIAN J. Pyramidal-cell plasticity in weakly electric fish: a mechanism for attenuating responses to reafferent electrosensory inputs. *J Comp Physiol [A]* 176: 63–73, 1995.

BASTIAN J. Plasticity in an electrosensory system. I. General features of a dynamic sensory filter. *J Neurophysiol* 76: 2483–2496, 1996a.

BASTIAN J. Plasticity in an electrosensory system. II. Postsynaptic events associated with a dynamic sensory filter. *J Neurophysiol* 76: 2497–2507, 1996b.

BASTIAN J. Plasticity in an electrosensory system III. Contrasting properties of spatially segregated dendritic inputs. *J Neurophysiol* 79: 1839–1857, 1998a.

BASTIAN J. Modulation of a calcium dependent postsynaptic depression contributes to an adaptive sensory filter. *J Neurophysiol* 80: 3352–3355, 1998b.

BASTIAN J. Plasticity of feedback inputs in the apteronotid electrosensory system. *J Exp Biol* 202: 1327–1337, 1999.

BERMAN NJ, DUNN RJ, AND MALER L. Function of NMDA receptors and persistent sodium channels in a feedback pathway of the electrosensory system. *J Neurophysiol* 86: 1612–1621, 2001.

BERMAN NJ AND MALER L. Interaction of $GABA_B$-mediated inhibition with voltage-gated currents of pyramidal cells: computational mechanism of a sensory searchlight. *J Neurophysiol* 80: 3197–3213, 1998a.

BERMAN NJ AND MALER L. Inhibition evoked from primary afferents in the electrosensory lateral line lobe of the weakly electric fish (*Apteronotus leptorhynchus*). *J Neurophysiol* 80: 3173–3196, 1998b.

BERMAN NJ, PLANT J, TURNER R, AND MALER L. Excitatory amino acid transmission at a feedback pathway in the electrosensory system. *J Neurophysiol* 78: 1869–1881, 1997.

BRATTON B AND BASTIAN J. Descending control of electroreception. II. Properties of nucleus praeeminentialis neurons projecting directly to the electrosensory lateral line lobe. *J Neurosci* 10: 1241–1253, 1990.

CHACRON MJ, LONGTIN A, AND MALER L. Negative interspike interval correlations increase the neuronal capacity for encoding time-dependent stimuli. *J Neurosci* 21: 5328–5343, 2001.

CRAMPTON WGR. Electric signal design and habitat preferences in a species rich assemblage of gymnotiform fishes from the upper Amazon basin. *Anais da Acad Brasileira de Ciencias* 70: 805–847, 1998.

CRICK F. Function of the thalamic reticular complex: the searchlight hypothesis. *Proc Natl Acad Sci USA* 81: 4586–5490, 1984.

DE KONINCK P AND SCHULMAN H. Sensitivity of CaM kinase II to the frequency of Ca^{2+} oscillations. *Science* 279: 227–230, 1998.

DELANEY KR AND TANK DW. Quantitative measurement of the dependence of short-term synaptic enhancement on presynaptic residual calcium. *J Neurosci* 14: 5885–5902, 1994.

DELANEY KR, ZUCKER RS, AND TANK DW. Calcium in motor nerve terminals associated with post tetanic potentiation. *J Neurosci* 9: 3558–3567, 1989.

DITTMAN JS, KREITZER AC, AND REGEHR WG. Interplay between facilitation, depression and residual calcium at three presynaptic terminals. *J Neurosci* 20: 1374–1385, 2000.

DITTMAN JS AND REGHER WG. Calcium dependence and recovery kinetics of presynaptic depression at the climbing fiber to Purkinje cell synapse. *J Neurosci* 18: 6147–6162, 1998.

FISCHER SA, FISCHER TM, AND CAREW TJ. Multiple overlapping processes underlying short-term synaptic enhancement. *Trends Neurosci* 20: 170–177, 1997.

GABBIANI F, METZNER W, WESSEL R, AND KOCH C. From stimulus encoding to feature extraction in weakly electric fish. *Nature* 384: 564–567, 1996.

HAN VZ, GRANT K, AND BELL C. Reversible associative depression and nonassociative potentiation at a parallel fiber synapse. *Neuron* 27: 611–622, 2000.

HANSON PI, MEYER T, STRYER L, AND SCHULMAN H. Dual role of calmodulin in autophosphorylation of multifunctional CaM kinase may underlie decoding of calcium signals. *Neuron* 12: 943–956, 1994.

HANSON PJ AND SCHULMAN H. Neuronal Ca^{2+}/calmodulin-dependent protein kinases. *Annu Rev Biochem* 61: 559–601, 1992.

HEMPEL CM, HARTMAN KH, WANG X-J, TURRIGIANO GG, AND NELSON SB. Multiple forms of short-term plasticity at excitatory synapses in rat medial prefrontal cortex. *J Neurophysiol* 83: 3031–3041, 2000.

HERRINGTON J, NEWTON KR, AND BOOKMAN RJ. *B PULSE CONTROL V4.5: IGOR XOPs for Patch Clamp Data Acquisition and Capacitance Measurements.* Miami, FL: 1995.

JENSEN K, JENSEN MS, AND LAMBERT JDC. Post-tetanic potentiation of GABAergic IPSCs in cultured rat hippocampal neurones. *J Physiol (Lond)* 519.1: 71–84, 1999.

LANNOO MJ AND LANNOO SJ. Why do electric fish swim backwards? An hypothesis based on gymnotiform behavior, interpreted through sensory constraints. *Environ Biol Fish* 36: 157–165, 1992.

LEWIS JE, OSWALD AM, AND MALER L. Dynamics of electrosensory feedback pathways and depth perception in weakly electric fish. *Soc Neurosci Abstr* 26: 567.12, 2000.

MAGLEBY KL AND ZENGEL JE. A dual effect of repetitive stimulation on post-tetanic potentiation of transmitter release at the frog neuromuscular junction. *J Physiol (Lond)* 245: 163–182, 1975.

MALER L, FINGER T, AND KATEN HJ. Differential projections of ordinary lateral line and electroreceptors in the gymnotiform fish *Apternotus albifrons. J Comp Neurol* 158: 363–382, 1974.

MALER L AND HINCKE M. The distribution of calcium/calmodulin-dependent kinase 2 in the brain of *Apteronotus leptorhynchus. J Comp Neurol* 408: 177–203, 1999.

MALER L, SAS EK, AND ROGERS J. The cytology of the posterior lateral line lobe of high frequency weakly electric fish (*Gymnotoidei*): differentiation and synaptic specificity in a simple cortex. *J Comp Neurol* 195: 87–139, 1981.

MATHIESON WB AND MALER L. Morphological and electrophysiological properties of a novel in vitro preparation: the electrosensory lateral line lobe brain slice. *J Comp Physiol [A]* 163: 489–506, 1988.

MATSUSHITA T, MORIYAMA S, AND FUKAI T. Switching dynamics and the transient memory storage in a model enzyme network involving Ca^{2+}/calmodulin-dependent protein kinase II in synapses. *Biol Cybern* 72: 497–509, 1995.

NELSON ME AND MACIVER MA. Prey capture in the weakly electric fish Apteronotus leptorhynchus: sensory acquisition strategies and electrosensory consequences. *J Exp Biol* 202: 1195–1203, 1999.

RATNAM R AND NELSON ME. Non-renewal statistics of electrosensory afferent spike trains: implications for the detection of weak sensory signals. *J Neurosci* 20: 6672–6683, 2000.

VARELA JA, SEN K, GIBSON J, FROST J, ABBOTT LF, AND NELSON SB. A quantitative description of short-term plasticity at excitatory synapses in layer 2/3 of rat primary visual cortex. *J Neurosci* 17: 7926–7940, 1997.

VARELA JA, SONG S, TURRIGIANO GG, AND NELSON SB. Differential depression at excitatory and inhibitory synapses in visual cortex. *J Neurosci* 19: 4293–4305, 1999.

WANG D AND MALER L. In vitro plasticity of the direct feedback pathway in the electrosensory system of *Apteronotus leptorhynchus. J Neurophysiol* 78: 1882–1889, 1997.

WANG D AND MALER L. Differential role of Ca^{2+}/calmodulin-dependent kinases in post tetanic potentiation at input selective glutamatergic pathways. *Proc Natl Acad Sci USA* 95: 7133–7138, 1998.

ZUCKER RS. Short-term synaptic plasticity. *Annu Rev Neurosci* 12: 13–31, 1989.